Journal of Solid State Electrochemistry (2019) 23:3019–3029
https://doi.org/10.1007/s10008-019-04397-0

ORIGINAL PAPER

Orthophosphoric acid solutions of sodium orthovanadate, sodium tungstate, and sodium molybdate as potential corrosion inhibitors of the Al_2Cu intermetallic phase

Przemysław Kwolek[1] · Kamil Dychtoń[1] · Maciej Pytel[1]

Received: 18 March 2019 / Revised: 7 September 2019 / Accepted: 8 September 2019 / Published online: 7 October 2019

Abstract
Orthophosphoric acid solutions of sodium orthovanadate, sodium tungstate, and sodium molybdate are tested as potential corrosion inhibitors of the Al_2Cu intermetallic phase. Corrosion inhibition is observed for 0.2 M solutions of Na_3VO_4 and Na_2WO_4 by increasing the pH to > 2. When the pH is < 2, the aforementioned salts increase the corrosion rate of the intermetallic phase. A 0.2 M solution of Na_3VO_4 causes the precipitation of vanadium phosphate on the surface of the Al_2Cu phase at pH = 1.

Keywords Intermetallics · Selective corrosion · Sodium molybdate · Sodium orthovanadate · Sodium tungstate · Heteropolyanions

Introduction

The intermetallic Al_2Cu phase is an important microstructural component of Al–Cu–Mg–Mn and Al–Zn–Mg–Cu wrought alloys because it ensures good strength by forming fine precipitates in the alloy matrix [1]. However, since it is nobler than the matrix, it promotes local dissolution and reduces the corrosion resistance of alloys [2, 3]. It is also well known that the formation of Al_2Cu plays an important role in many Al–Cu-based cast alloys [4–9]. The distribution of the Al_2Cu phase in the interdendritic spacing affects both the mechanical and corrosion behaviour of the alloys [4–7]. This effect is not proportional, meaning that the microstructural refinement level and the cathode-to-anode area ratio strongly affect the mechanical-to-corrosion response [4, 8, 9]. At the same time, the intermetallic Al_2Cu phase is itself susceptible to selective corrosion, and when immersed in acidic, neutral, and alkaline solutions, its surface is transformed into a highly porous metallic copper [2, 10].

The corrosion and wear resistance of components containing aluminium alloys can be improved by an appropriate surface treatment, which often requires acid etching, such as in the stripping of anodic coatings. In this case, a corrosion inhibitor is required for the metallic substrate, such as commonly used chromium trioxide [11]. However, due to its toxicity, new environmentally friendly inhibitors that are usable in acidic solutions must be developed, which requires understanding their influence on the corrosion behaviour of both the alloy and its microstructural constituents.

In this work, three inorganic salts, namely sodium orthovanadate (Na_3VO_4), sodium tungstate (Na_2WO_4) and sodium molybdate (Na_2MoO_4), were tested as potential corrosion inhibitors of the intermetallic Al_2Cu phase. A 0.5 M solution of orthophosphoric acid (H_3PO_4) was used as the corrosive environment because it is used in practice to strip anodic coatings [12].

The chemistry of the transition metals vanadium, niobium, tantalum, molybdenum and tungsten, in their highest oxidation states in aqueous solutions is very complex. When adding increasing amounts of a mineral acid to aqueous solutions of orthometalates (aka monometalates), addition and condensation processes progress and isopolyoxoanions are formed. They are built by a transition metal, oxygen and hydrogen. For the various equilibria, the resulting isopolyoxoanions are categorised in terms of their stoichiometric coefficients as described by the general equation (Eq. (1)):

$$pMO_4^{2-} + qH^+ \rightarrow \left[M_pO_{4p-q/2}\right]^{(2p-q)-} + \frac{q}{2}H_2O \quad (1)$$

✉ Przemysław Kwolek
pkwolek@prz.edu.pl

[1] Department of Materials Science, Rzeszow University of Technology, Rzeszów, Poland

where M = V, Nb, Ta, Mo or W. The degree of protonation Z of a particular species is defined by the ratio q/p. Heteropolyoxoanions incorporate one or more elements, in addition to the transition metal, oxygen and hydrogen.

The corrosion inhibition of aluminium alloys using isopolyoxovanadates was extensively studied in NaCl solutions [13–17]. In the mildly acidic solutions at low vanadate concentrations, tetrahedrally coordinated species, such as $[H_2VO_4]^-$ and $[V_4O_{12}]^{4-}$, inhibited the cathodic process [14]. Decavanadate ions, such as $[HV_{10}O_{28}]^{5-}$ and $[H_2V_{10}O_{28}]^{4-}$, which are stable in mildly and strongly acidic solutions, do not exhibit an inhibiting effect on the 2024 alloy [13, 14]. Tetrahedrally coordinated isopolyoxovanadates decrease the corrosion potential and corrosion current density of intermetallic Al_2Cu in 0.5 M NaCl solutions (pH = 9.17) and increase the pitting potential with little influence on the current density in the passive region of the anodic polarisation curve [15].

Isopolyoxotungstates were tested as corrosion inhibitors of aluminium in neutral and acidic solutions [18, 19]. Again, several stable species in aqueous solutions are possible, but the most common are paratungstate-A $[W_7O_{24}]^{6-}$ and metatungstate $[\alpha\text{-}H_2W_{12}O_{40}]^{6-}$ [20]. In acidic solution, isopolyoxotungstates increase the anodic and cathodic overpotentials and thus decrease the corrosion rate of Al, but the inhibition efficiency is low (ca. 50%) [19]. In a 0.5 M NaCl solution, these species increase the pitting potential of aluminium due to adsorption at flawed areas and developing pits [18].

Isopolyoxomolybdates have rarely been tested as potential corrosion inhibitors of aluminium in acidic solutions. The most important isopolyoxomolybdates that can be formed are dimolybdate $[Mo_2O_7]^{2-}$, trimolybdate $[Mo_3O_{10}]^{2-}$, tetramolybdate $[Mo_4O_{13}]^{2-}$, heptamolybdate (also called paramolybdate) $[Mo_7O_{24}]^{6-}$, octamolybdate $[Mo_8O_{26}]^{4-}$ and decamolybdate $[Mo_{10}O_{34}]^{8-}$; also, many large clusters, such as $[Mo_{36}O_{112}(H_2O)_{16}]^{8-}$, $[Mo_{154}(NO)_{14}O_{420}(OH)_{28}(H_2O)_{70}]^{25-}$ and $Na_{48}[H_xMo_{368}O_{1032}(H_2O)_{240}(SO_4)_{48}]\cdot$ca. $1000H_2O$ ($x \approx 16$), can be formed [20–23]. Regarding their inhibiting properties, it was demonstrated that in 1 M HCl, isopolyoxomolybdates increased the corrosion rate of aluminium [24], but in a chloride-free borate buffer (possibly containing a small amount of H_3PO_4), the corrosion rate of aluminium and its alloys decreased. It was concluded that isopolyoxomolybdates behaved as passivators when Mo atoms were incorporated into the surface film [25].

Heteropolyoxoanions can be formed by about 60 elements on the periodic table, but one of the most important is phosphorus. Vanadium forms heteropolyoxoanions less frequently than molybdenum and tungsten, and known species include $[PV_{14}O_{42}]^{9-}$ and $[H_6PV_{13}O_{41}]^{7-}$ [20]. The most notable example of a heteropolyoxotungstate is $[PW_{12}O_{40}]^{3-}$; however, in the presence of excess H_3PO_4, which occurs when sodium tungstate is used as the corrosion inhibitor in orthophosphoric acid, $[P_4W_8O_{40}]^{12-}$ can be formed [20]. Neither heteropolyoxovanadates nor heteropolyoxotungstates have been tested as corrosion inhibitors of aluminium; thus, heteropolyoxomolybdates are somewhat exceptional from this point of view. The most well-known heteropolyoxomolybdate is $[PMo_{12}O_{40}]^{3-}$, which is a more powerful oxidant than $[PW_{12}O_{40}]^{3-}$ and can be easily reduced to phosphomolybdenum blue species $[PMo_{12}O_{40}]^{7-}$, which are widely used in analytical chemistry [26]. The corrosion inhibition of aluminium and 2024 aluminium alloy in the H_3PO_4–Na_2MoO_4 system has been demonstrated [24, 27–29]. Interestingly, iso- and heteropolyoxomolybdates also decrease the dissolution rate of anodic coatings in solutions of orthophosphoric acid [30].

Experimental

Al_2Cu electrodes were obtained by an electrical arc melting process in water-cooled copper crucibles using a tungsten electrode under an Ar atmosphere (p = 60 kPa). Stoichiometric amounts of Al and Cu (99.999 wt% purity, Alfa Aesar) were weighed to obtain approximately 4.5 g of the alloy with a theoretical Cu content of 53.4 wt%. The feedstock material was re-melted four times to obtain a homogeneous material. A small amount of a eutectic mixture of Al_2Cu and Al(Cu) solid solution crystals was obtained together with the hypereutectic crystals of the Al_2Cu phase. The former was dissolved during subsequent heat treatment in air (T = 823 K, t = 30 h). X-ray diffraction confirmed that Al_2Cu was obtained (International Centre for Diffraction Data (ICDD) card 04-001-0923). Subsequently, the specimens were cut using an electrical discharge machine and mounted in an epoxy resin. The surface area of the electrodes was approximately 0.79 cm^2. Prior to the corrosion tests, they were abraded by SiC papers (320 and 500 grit), washed with water and isopropyl alcohol, and then dried with flowing air.

Corrosion tests were performed in a conventional three-electrode electrochemical cell open to air with a water jacket and equipped with platinum counter electrodes (20 cm^2). The reference electrode (Ag/AgCl in 3 M KCl) was placed in a Luggin probe filled with 1 M KNO_3 solution. The volume of tested solutions was 100 cm^3 at a temperature T of 303 K. The electrochemical cell was placed in a Faraday cage and connected to a Bio-Logic SP-300 potentiostat.

Na_3VO_4, Na_2WO_4 and Na_2MoO_4 were dissolved in 0.5 M orthophosphoric acid. Concentrations equal to 10, 50, 100 and 200 mM were obtained. The open-circuit potential (OCP) of Al_2Cu was recorded for 10 h, and within this period, the impedance spectra were measured. The first one was obtained at t = 20 min, and subsequent ones were obtained every 2 h. The frequency domain of the spectra was between 200 kHz and 10 mHz with 5 mV of a root mean square (RMS) of sinusoidal perturbation of potential. The impedance spectra were validated using a Kramers-Kronig transformation (KK Test software)

[31, 32]. Only spectra obtained under stationary conditions are presented in this work. They were approximated using the appropriate equivalent circuit in Zview software (Scribner Associates). Values of the fitted parameters were normalised to the geometric surface area of the specimen, i.e. 0.79 cm^2. The quality of the fit was estimated using two parameters: χ^2 (chi squared) and *S*. The former, in the Zview software, is defined as the square of the standard deviation between the measured and calculated data. The latter is the weighted sum of squares of differences between measured and calculated data, where the weighting factors are the moduli of calculated impedances.

The influence of pH on the corrosion kinetics of the Al_2Cu phase was established based on additional corrosion experiments. The following solutions were used: 0.5 M H_3PO_4/0.2 M Na_3VO_4 and 0.5 M H_3PO_4/0.2 M Na_2WO_4 at pH 1.0 as well as 0.5 M Na_3PO_4 at pH 2.2 and 3.9. The pH was adjusted using concentrated H_2SO_4.

The aluminium and copper concentrations in solutions after corrosion tests were measured using inductively coupled plasma-optical emission spectroscopy ICP-OES (Ultima 2 Horiba Jobin Yvon). Due to a significant matrix effect, the standard addition method was applied. The morphology and chemical composition of the surface of corroded Al_2Cu specimens were determined using scanning electron microscopy (SEM) on a HITACHI S-3400N equipped with energy-dispersive X-ray spectrometer (EDX) (Thermo Noran System 7).

Results and discussion

Corrosion rate of intermetallic Al_2Cu

Sodium orthovanadate, sodium molybdate and sodium tungstate form isopolyoxoanions and heteropolyoxoanions when they are dissolved in orthophosphoric acid solution. They were tested as corrosion inhibitors of intermetallic Al_2Cu. The concentration of aluminium c_{Al} and copper c_{Cu} in the solution was determined as a function of the initial concentration of the monometalates after 10 h of immersion (Fig. 1). The intermetallic phase in the acidic solution was susceptible to selective corrosion. Aluminium atoms were preferentially dissolved, and the electrode surface was enriched with copper and became porous. In 0.5 M H_3PO_4, for instance, c_{Al} was approximately 300-fold higher than c_{Cu}. Thus, it can be concluded that the c_{Al}/c_{Cu} depends on the added inorganic salt and its initial concentration.

Sodium orthovanadate, when used at a low concentration (10 mM), significantly increased the corrosion rate of the intermetallic phase (Fig. 1a). However, when its concentration was ≥ 100 mM, it inhibited the corrosion process. Additionally, under such conditions, the Al_2Cu phase did not selectively corrode. Sodium tungstate influenced the corrosion kinetics of the intermetallic phase in a similar manner. However, it was a less efficient inhibitor than Na_3VO_4 (Fig. 1b). Interestingly, when its concentration was < 200 mM, a white powder precipitated, along with the corrosion of the intermetallic phase. However, the powder contained neither aluminium nor copper and was mainly composed of tungsten (ca. 17 at%) and oxygen with a small admixture of phosphorus and sodium. Thus, it was likely one of the heteropolyoxotungstate forms. Sodium molybdate, in turn, increased the corrosion rate of the Al_2Cu phase in the whole studied concentration range (10–200 mM) and was excluded from further analysis.

On the one hand, the monometalates Na_3VO_4 and Na_2WO_4, when dissolved in an acid, increase its pH. On the other hand, the Al_2Cu phase is passive over a wide pH range between 2 and 10 [33]. Therefore, understanding the corrosion behaviour of Al_2Cu required determining the pH of the solutions prior to the corrosion experiments (Fig. 2). The corrosion inhibition may be related to an increase in the pH of the solutions. This possibility was further explored using electrochemical impedance spectroscopy (EIS).

Electrochemical analysis

The corrosion kinetics of the Al_2Cu phase was studied in 0.5 M H_3PO_4, 0.5 M H_3PO_4/0.01 M Na_3VO_4 and 0.5 M H_3PO_4/0.2 M Na_3VO_4 at pH = 1.0, 1.3 and 3.9, respectively, as well as 0.5 M H_3PO_4/0.05 M Na_2WO_4 and 0.5 M H_3PO_4/0.2 M Na_2WO_4 at pH = 1.2 and 2.2, respectively. Additional corrosion tests were performed in 0.5 M H_3PO_4/0.2 M Na_3VO_4 and 0.5 M H_3PO_4/0.2 M Na_2WO_4 acidified to pH = 1.0 as well as 0.5 M Na_3PO_4 acidified to pH = 3.9 and 2.2.

Immediately after immersion in acidic solution, the Al_2Cu corroded via hydrogen and oxygen depolarisation. The appearance of the electrode surface changed from shiny to dull and copper-like, which was caused by the selective dissolution of aluminium atoms. The porous structure, composed of Cu, was formed on the surface of the electrode (Fig. 3a). The open-circuit potential of the electrode increased with time (Fig. 4a). When it was > − 267 mV vs. a Ag/AgCl reference electrode (equilibrium potential of standard hydrogen electrode at pH = 1), the corrosion mechanism changed to oxygen depolarisation. The same mechanism was responsible for corrosion of Al_2Cu in 0.5 M H_3PO_4/0.01 M Na_3VO_4 and 0.5 M H_3PO_4/0.05 M Na_2WO_4. When the initial concentration of sodium orthovanadate was equal to 0.2 M, the open-circuit potential achieved the highest value. The OCP was relatively low, in turn, in 0.5 M H_3PO_4/0.2 M Na_2WO_4 at pH = 1.0 (Fig. 4b).

Electrochemical impedance spectroscopy was used to study the influence of the chemical composition of the solutions on the corrosion mechanism of Al_2Cu. First, the modulus of the imaginary part of impedance was analysed as a

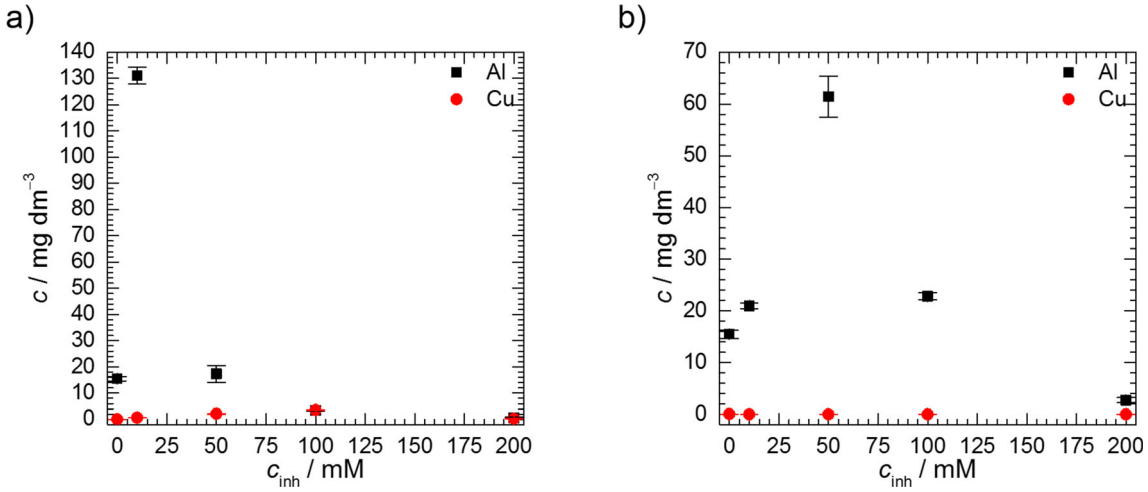

Fig. 1 Concentration of Cu and Al in 0.5 M H_3PO_4 solutions after t = 10 h immersion of intermetallic Al_2Cu, T = 303 K, as a function of the initial concentration of **a** Na_3VO_4 and **b** Na_2WO_4

function of frequency (Fig. 5). It can be observed that in the high-frequency range > 10 kHz, $|Z''|$ decreased as the frequency decreased. It is usually regarded as an artefact related to the impedance of the reference electrode, stray capacitance from the cable connected to the voltage amplifier and its input capacitance [34]. Therefore, this frequency range was excluded from the approximation. However, Orazem et al. observed and discussed similar behaviour for selectively corroded cast iron. In their results, the high-frequency part of the spectrum, in the form of the incomplete capacitive loop in the Nyquist plot, was related to the microporous film present on the surface of the cast iron and the cathodic charge-transfer process [35].

A subsequent linear increase in log $|Z''|$ can be observed for the selectively corroded Al_2Cu phase, usually between 70 kHz and 100 Hz (Fig. 5) [35]. The impedance spectra of such porous electrodes can be approximated using the de Levie model; however, the important parameters characterizing the electrochemical process, such as the charge-transfer resistance R_{ct} and the double-layer capacitance C_{dl}, cannot be estimated easily [36]. Lasia et al. proposed a so-called two CPE model, in which a high-frequency capacitive loop is related to a porous film on the surface of the electrode and a low-frequency loop is related to its corrosion [37, 38]. In our case, however, using the "two CPE" model gave high approximation errors of the electrical equivalent circuit (EEC) elements. Therefore, the high-frequency range of the impedance spectra was not approximated. Only in the case of a solution containing 200 mM Na_3VO_4 at pH = 1.0 was a well-established capacitive loop in this range of frequencies visible.

Another straight line in Fig. 5 can be observed over a wide range of frequencies down to ca. 1 Hz. This corresponds to the double-layer capacitance C_{dl} connected in parallel to the charge-transfer resistance R_{ct}. However, due to the frequency dispersion, the negative value of the slope is < 1; thus, a constant phase element (CPE_{dl}) was used instead of a capacitor in the EEC (Figs. 6 and 8). The impedance of the CPE is given by Eq. (2) [39, 40]:

$$Z_{CPE} = \frac{1}{T(j\omega)^{\alpha}} \tag{2}$$

where T is the parameter related to the electrode capacitance, ω is the angular frequency and α indicates the deviation from purely capacitive behaviour. When $\alpha = 1$, T equals the capacitance. It seems reasonable that time constants for the faradaic process were distributed along, rather than normal to, the surface of the electrode. Thus, the following equation can be applied to obtain the double-layer capacitance C_{dl} (Eq. (3)) [40–42]:

$$C_{dl} = T_{dl}^{\frac{1}{\alpha}} \left(\frac{R_s R_{ct}}{R_s + R_{ct}} \right)^{\frac{1-\alpha}{\alpha}} \tag{3}$$

where R_s is the solution resistance, R_{ct} is the charge-transfer resistance, T_{dl} is the parameter of the constant phase element representing the electrical double layer and α is the exponent

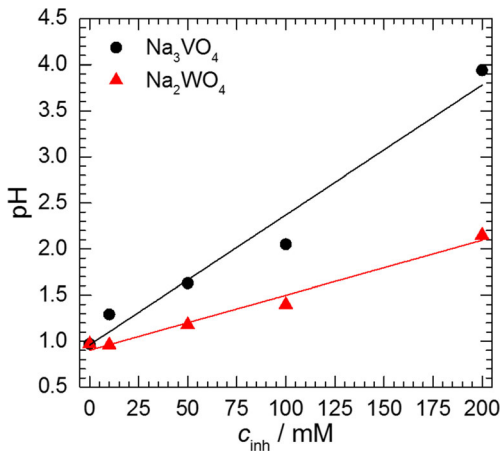

Fig. 2 The pH of the solutions of Na_3VO_4 and Na_2WO_4 in 0.5 M H_3PO_4

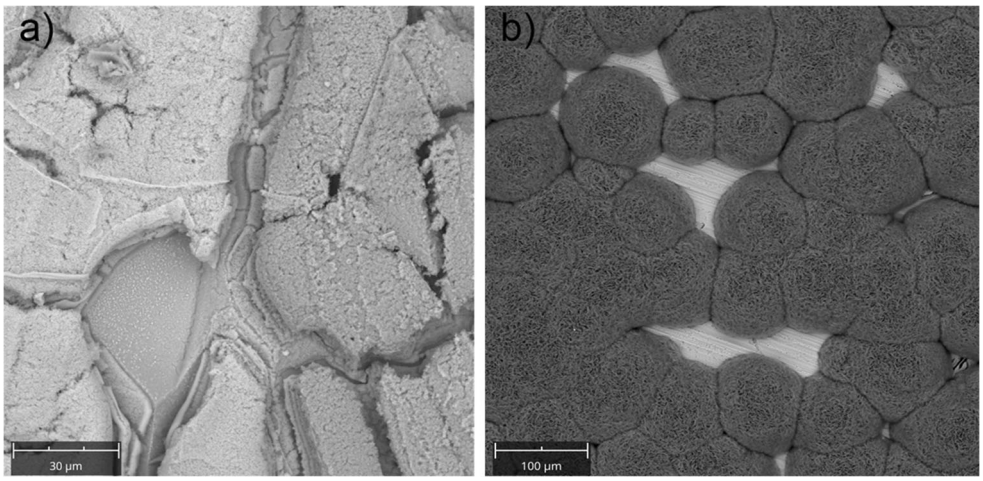

Fig. 3 Scanning electron micrograph of the Al_2Cu surface after 10 h exposure in **a** 0.5 M H_3PO_4 and **b** 0.5 M H_3PO_4/0.2 M Na_3VO_4 at pH = 1.0 and T = 303 K

of the CPE. It should be noted here that when $\alpha < 0.85$, calculation of C_{dl} using Eq. (3) can lead to significant error [43].

An additional time constant was observed for frequencies < 1 Hz. The inductive behaviour in the Nyquist plots (e.g. Fig. 6a) was approximated by the inductor L_1 in series with a resistor R_1. These are related to the adsorption of intermediate species due to the anodic dissolution of metal and/or corrosion inhibitor species [40]. The same model can be applied to a passive electrode. The resistance then takes into account the kinetics of changes to the fractional surface coverage or film resistivity with time, whereas inductance is related to the time constant of this process [44]. The low-frequency inductive behaviour of corroding metal is frequently observed (e.g., [24, 45] and [46] in the case of aluminium in acidic solutions and intergranular corrosion of stainless steel, respectively).

In the case of 200 mM Na_3VO_4 at pH = 3.9, the inductor-containing equivalent circuit was not applicable. A much better approximation was achieved using the alternative model for the passive electrode, where a constant phase element was applied instead of a capacitor (Fig. 6b) [40]. The physical meaning of CPE_1 and R_2 is not straightforward, but they are related to the charge-transfer resistance, the change in the electric current passing through the interface caused by a change in the fractional coverage of the surface, film resistivity, or thickness, as well as the time constants related to these processes [40]. An additional time constant, visible for 200 mM Na_3VO_4 at pH = 1.0 (Fig. 5) for f < 100 mHz, was not approximated.

The impedance spectra obtained for the Al_2Cu phase in the solutions without corrosion inhibitors at pH ≥ 2.2 (0.5 M Na_3PO_4) were well approximated with a simple, Randles-type equivalent circuit (Figs. 5 and 6c, d).

The impedance spectra obtained for the corrosion of Al_2Cu in 0.5 M H_3PO_4/0.2 M Na_2WO_4 and 0.5 M H_3PO_4/0.2 M Na_3VO_4 with their approximation using an electrical equivalent circuit are presented in Fig. 6a, b, respectively. Relatively high values of the impedance, especially for the sodium

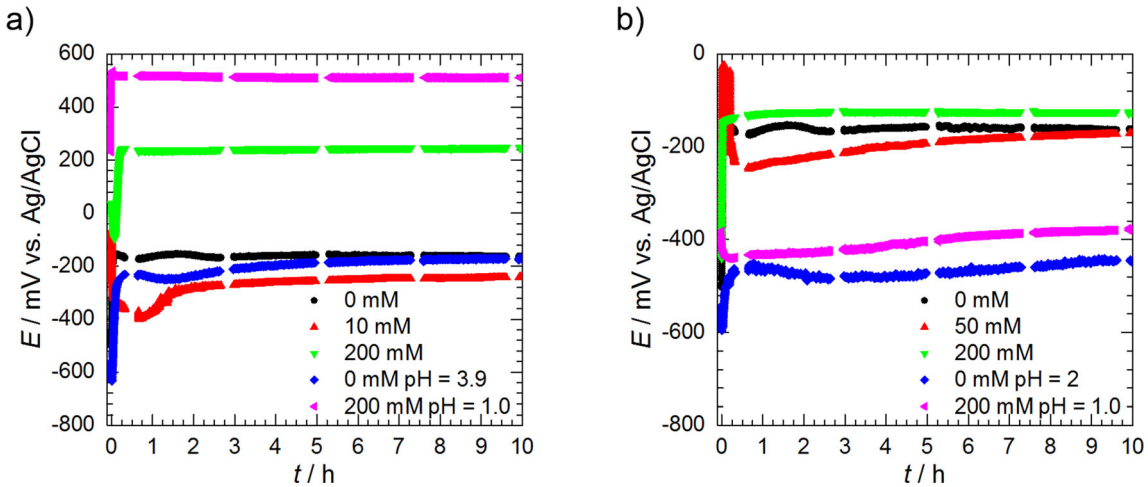

Fig. 4 Open-circuit potential of Al_2Cu in 0.5 M H_3PO_4 at T = 303 K as a function of time, pH and initial concentration of **a** sodium orthovanadate and **b** sodium tungstate

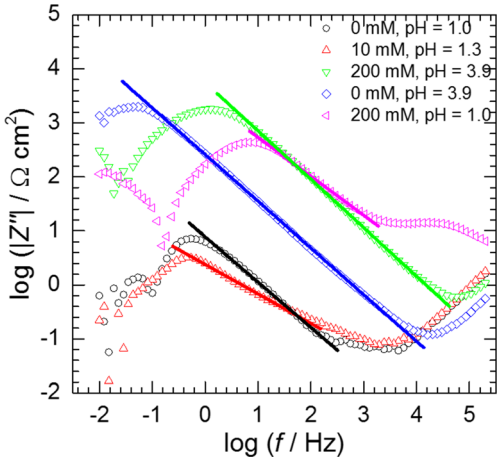

Fig. 5 Modulus of the imaginary part of impedance as a function of frequency for Al_2Cu exemplary corrosion processes in the presence of Na_3VO_4; impedances were multiplied by the geometric surface area

orthovanadate, suggest efficient corrosion inhibition. However, similarly high impedances were obtained for the Al_2Cu in 0.5 M Na_3PO_4 acidified to pH = 2.2 and 3.9 (Fig. 6c, d).

The double-layer capacitance calculated for the Al_2Cu phase immersed in 0.5 M Na_3PO_4 at pH = 2.2 was very high when compared to the typical value for smooth metal surfaces (20 μF cm^{-2}) [37] and increased with time from 2195 to 6389 μF cm^{-2}. Lasia reported even higher values that reached 2.4 F cm^{-2} [37, 38]. This is related to the enormous increase of surface area of the electrode caused by the selective dissolution of Al (Fig. 3a). The double-layer capacitance increases with time as the surface area of the electrode increases. In this work, capacitances were divided by the geometric surface area, i.e. 0.79 cm^2. The real value, however, changes with time and can be between several hundred and several thousand times higher when compared to the initial value. The exact value remains unknown. Therefore, the increase of C_{dl} with time is observed. In fact, it is only related to the aggressiveness of the corrosive environment.

For 200 mM of Na_2WO_4 in turn, the double-layer capacitance was equal to ca. 190 μF cm^{-2} and did not change with

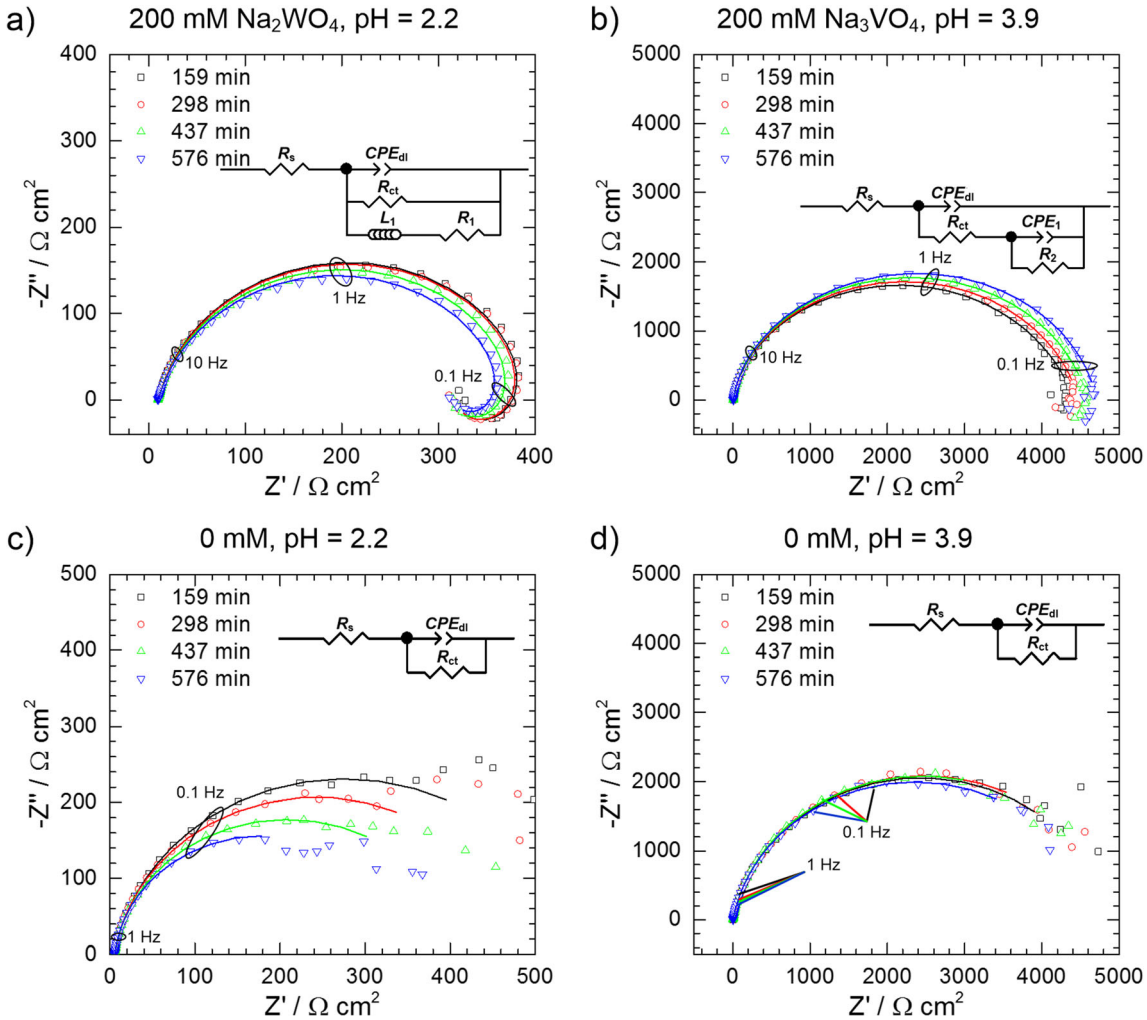

Fig. 6 Nyquist plots for the corrosion of Al_2Cu as a function of time in **a**, **b** 0.5 M H_3PO_4 and **c**, **d** 0.5 M Na_3PO_4 at $T = 303$ K; continuous lines represent an approximation of the obtained data, impedances were multiplied by the geometric surface area

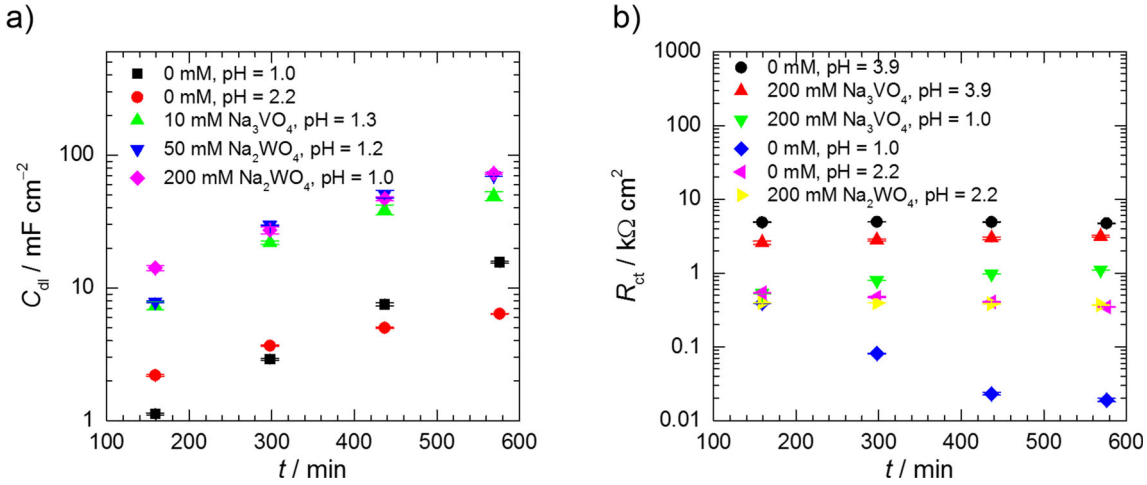

Fig. 7 Corrosion kinetics of Al_2Cu in 0.5 M H_3PO_4 at $T = 303$ K for the exemplary chemical composition of the solutions: **a** double-layer capacitance and **b** charge-transfer resistance; capacitances were divided and resistances multiplied by the geometric surface area

time. Analogously, the charge-transfer resistance after t = 576 min was high for the solution containing Na_2WO_4 (370 vs 347 Ω cm^2, Table 1). It indicates that there was no such a severe dealloying of the intermetallic phase as described above. The corrosion rate was calculated based on the concentration of aluminium c_{Al} and copper c_{Cu} in the solution and was equal to 21.58 and 8.27 g m^{-2} day^{-1} for 0.5 M Na_3PO_4 and 0.5 M H_3PO_4/0.2 M Na_2WO_4, respectively, at pH = 2.2. Thus, a rather weak inhibition effect was achieved with an inhibition efficiency equal to 62%.

The inhibition effect was not observed for pH = 3.9 in 0.5 M H_3PO_4/0.2 M Na_3VO_4. The corrosion rate of the Al_2Cu phase was higher when compared to the solution without this salt at the same pH (2.61 g m^{-2} day^{-1} with the Na_3VO_4 and 2.34 g m^{-2} day^{-1} without the Na_3VO_4). The charge-transfer resistance was also higher for the solution without sodium orthovanadate (Fig. 7b). The double-layer capacitance, calculated for the Al_2Cu phase immersed in 0.5 M H_3PO_4/0.2 M Na_3VO_4, was between 12 and 14 μF cm^{-2}, which is close to the value typical for smooth metal surfaces (20 μF cm^{-2}) [37]. Interestingly, much higher values, between 200 and 350 μF cm^{-2}, were obtained for the Al_2Cu phase at pH = 3.9 in the solution without sodium orthovanadate when there was no selective corrosion. The same effect was reported in the literature for Al_2Cu immersed in 0.1 M NaCl solution. The high electrical double-layer capacitance was attributed to the formation of hydroxide ions on the surface due to the oxygen reduction reaction [47].

0.5 M H_3PO_4/0.2 M Na_3VO_4 and 0.5 M H_3PO_4/0.2 M Na_2WO_4 solutions were then acidified to pH = 1.0. The impedance spectra of the Al_2Cu were compared with those obtained for 0.5 M H_3PO_4 (Fig. 8). It can be seen that sodium tungstate, when dissolved in orthophosphoric acid at pH = 1, increased the corrosion rate of the intermetallic phase. High values of the double-layer capacitance indicate selective corrosion (Fig. 7a). The charge-transfer resistance decreased with time from 51 to 19 Ω cm^2 (Table 1). The corrosion rate is 3-fold higher when compared to that of a 0.5 M H_3PO_4 solution.

In the case of sodium orthovanadate (200 mM, pH = 1.0), the values of R_{ct}, L_1 and R_1 increased with time (Table 1; Fig. 7b), whereas C_{dl} only slightly increased between 9 and 12 μF cm^{-2}. This was caused by the formation of the protective layer on the Al_2Cu surface. The layer was composed mainly of vanadium, phosphorus, oxygen and sodium, where the P/V atomic ratio was close to unity. The high-frequency capacitive loop (f > 1 kHz), emerging at the impedance spectra (Fig. 8d), was related to the microporosity of this layer. However, the corrosion protection was only moderate, since the areas uncovered can be easily found on the surface (Fig. 3b). The corrosion rate of Al_2Cu in 0.5 M H_3PO_4 was 47.12 g m^{-2} day^{-1} and decreased to 39.93 g m^{-2} day^{-1} in the solution containing initially 200 mM of Na_3VO_4.

The most severe Al_2Cu corrosion occurred in 0.5 M H_3PO_4/0.01 M Na_3VO_4 (pH = 1.3), 0.5 M H_3PO_4/0.05 M Na_2WO_4 (pH = 1.2) and 0.5 M H_3PO_4/0.2 M Na_2WO_4 (pH = 1.0) since the pH was strongly acidic, and the species formed in the solution acted as additional depolarisers in the corrosion cell. The surface area of these electrodes increased with time and was 1–3.5 thousand times higher when compared to the smooth surface (assumed capacitance 20 μF cm^{-2} [37]). Thus, the highest values of the double-layer capacitance among the samples in this study were obtained (Fig. 7a). It should be noted here that fitted values of α were < 0.85 for 200 mM Na_2WO_4, pH = 1, t = 159, 298, 437 and 576 min as well as 10 mM Na_3VO_4, pH = 1.3, t = 437 and 576 min. Thus, the errors of C_{dl} values in these cases can be significant [43]. The charge-transfer resistance, for selectively corroded specimens, decreased with time due to increase of the real surface area, and after 10 h, reached low values between 10 and 30 Ω cm^2. This is not related with the change of corrosion mechanism. R_{ct} values presented in Table 1 were multiplied by the geometric surface area.

Table 1 The results of the approximation of the impedance spectra, where χ^2 and S indicate the quality of the fit (chi-square and residual sum of squares, respectively); R_s is the solution resistance; T_{dl} is the constant phase element parameter representing the electrical double layer; α_{dl} is the exponent of the CPE; R_{ct} is the charge-transfer resistance; L_1 and R_1 are the inductance and resistance related to the adsorption processes onto the electrode, respectively; T_1 and α_1 are the parameter and exponent of CPE_1, respectively; R_2 is the resistance, which is related to the passive layer formed onto Al_2Cu; and Δ indicates the standard deviation of the aforementioned parameters; values of the fitted parameters are normalised to geometric surface area of the specimen

c_{inh} (mM)	t (min)	χ^2	S	R_s (Ω cm^2)	ΔR_s	T_{dl} (μF s$^{\alpha-1}$ cm^{-2})	ΔT_{dl}	α_{dl}	$\Delta\alpha_{dl}$	R_{ct} (Ω cm^2)	ΔR_{ct}	L_1 (H cm^2)	ΔL_1	R_1 (Ω cm^2)	ΔR_1	T_1 (μF s$^{\alpha-1}$ cm^{-2})	ΔT_1	α_1	$\Delta\alpha_1$	R_2 (Ω cm^2)	ΔR_2
0 mM, pH = 1.0	159	6.78×10^{-4}	0.04	9	1	1439	13	0.95	0.01	393	5	1203	65	711	18						
	298	6.24×10^{-4}	0.04	8	1	3597	34	0.94	0.01	81	1	1538	112	277	27						
	437	1.59×10^{-4}	0.01	8	1	11,004	119	0.88	0.01	23	1	131	8	63	5						
	596	3.30×10^{-5}	0.01	8	1	21,795	164	0.87	0.01	19	1	56	2	43	1						
0 mM, pH = 2.2	159	1.05×10^{-3}	0.07	6	1	3414	22	0.90	0.01	540	7										
	298	6.37×10^{-4}	0.04	6	1	5152	24	0.91	0.01	474	5										
	437	6.62×10^{-4}	0.05	6	1	6763	29	0.92	0.01	405	4										
	576	2.56×10^{-4}	0.02	6	1	8002	25	0.93	0.01	347	3										
0 mM, pH = 3.9	159	5.14×10^{-4}	0.05	5	1	418	1	0.89	0.01	4859	31										
	298	2.33×10^{-4}	0.02	5	1	545	1	0.89	0.01	4931	24										
	437	1.94×10^{-4}	0.02	5	1	613	1	0.90	0.01	4906	26										
	596	1.81×10^{-4}	0.02	5	1	680	1	0.90	0.01	4702	21										
10 mM Na_3VO_4	159	2.28×10^{-4}	0.01	9	1	11,386	337	0.86	0.01	21	1	18	2	42	2						
	298	6.67×10^{-5}	0.01	9	1	28,929	435	0.87	0.01	14	1	23	1	24	1						
	437	1.46×10^{-4}	0.01	9	1	52,971	2233	0.80	0.01	13	1	12	2	21	2						
	596	1.40×10^{-4}	0.01	9	1	67,534	2491	0.78	0.01	11	1	13	2	21	2						
50 mM Na_2WO_4	159	1.31×10^{-4}	0.01	11	1	10,706	69	0.88	0.01	45	1	139	4	65	1						
	298	2.70×10^{-5}	0.01	11	1	35,697	151	0.86	0.01	36	1	57	1	39	1						
	437	1.69×10^{-3}	0.13	11	1	55,946	2247	0.89	0.01	30	1	50	15	50	12						
	576	6.67×10^{-4}	0.04	11	1	74,851	848	0.89	0.01	28	1	41	9	56	2						
200 mM Na_2WO_4 pH = 2.2	159	6.19×10^{-4}	0.06	10	1	449	4	0.86	0.01	396	2	4910	287	1481	76						
	298	6.83×10^{-4}	0.07	10	1	447	4	0.86	0.01	395	2	4490	237	1441	45						
	437	7.66×10^{-4}	0.07	10	1	462	4	0.85	0.01	384	2	4847	317	1519	73						
	576	8.85×10^{-4}	0.09	10	1	513	5	0.84	0.01	370	2	7078	568	1880	96						
200 mM Na_2WO_4 pH = 1.0	159	2.30×10^{-4}	0.02	6	1	28,362	1	0.73	0.01	51	3	47	4	65	3						
	298	3.0×10^{-4}	0.02	6	1	42,314	3	0.77	0.01	37	4	33	5	51	6						
	437	2.23×10^{-4}	0.01	6	1	62,895	2	0.80	0.01	22	1	68	12	59	7						
	576	5.02×10^{-5}	0.01	6	1	88,775	1	0.82	0.01	19	1	85	11	54	4						
200 mM Na_3VO_4 pH = 1.0	159	6.54×10^{-4}	0.05	11	1	41	2	0.84	0.01	532	2	3406	311	4236	322						
	298	6.03×10^{-4}	0.05	27	1	38	2	0.84	0.01	796	3	10,674	831	5461	449						
	437	4.84×10^{-4}	0.04	41	1	38	2	0.84	0.01	976	3	14,718	1242	7813	658						
	576	3.51×10^{-4}	0.03	52	1	38	2	0.85	0.01	1110	3	17,085	1455	10,558	770						
200 mM Na_3VO_4 pH = 3.9	159	2.87×10^{-4}	0.04	9	1	27	1	0.93	0.01	2585	118					107	10	0.68	0.01	1831	133
	298	3.15×10^{-4}	0.04	9	1	28	1	0.93	0.01	2799	106					111	10	0.73	0.01	1679	120
	437	3.63×10^{-4}	0.05	9	1	28	1	0.93	0.01	2958	118					110	12	0.75	0.01	1630	134
	569	3.86×10^{-4}	0.05	9	1	27	1	0.92	0.01	3136	106					111	11	0.78	0.01	1574	118

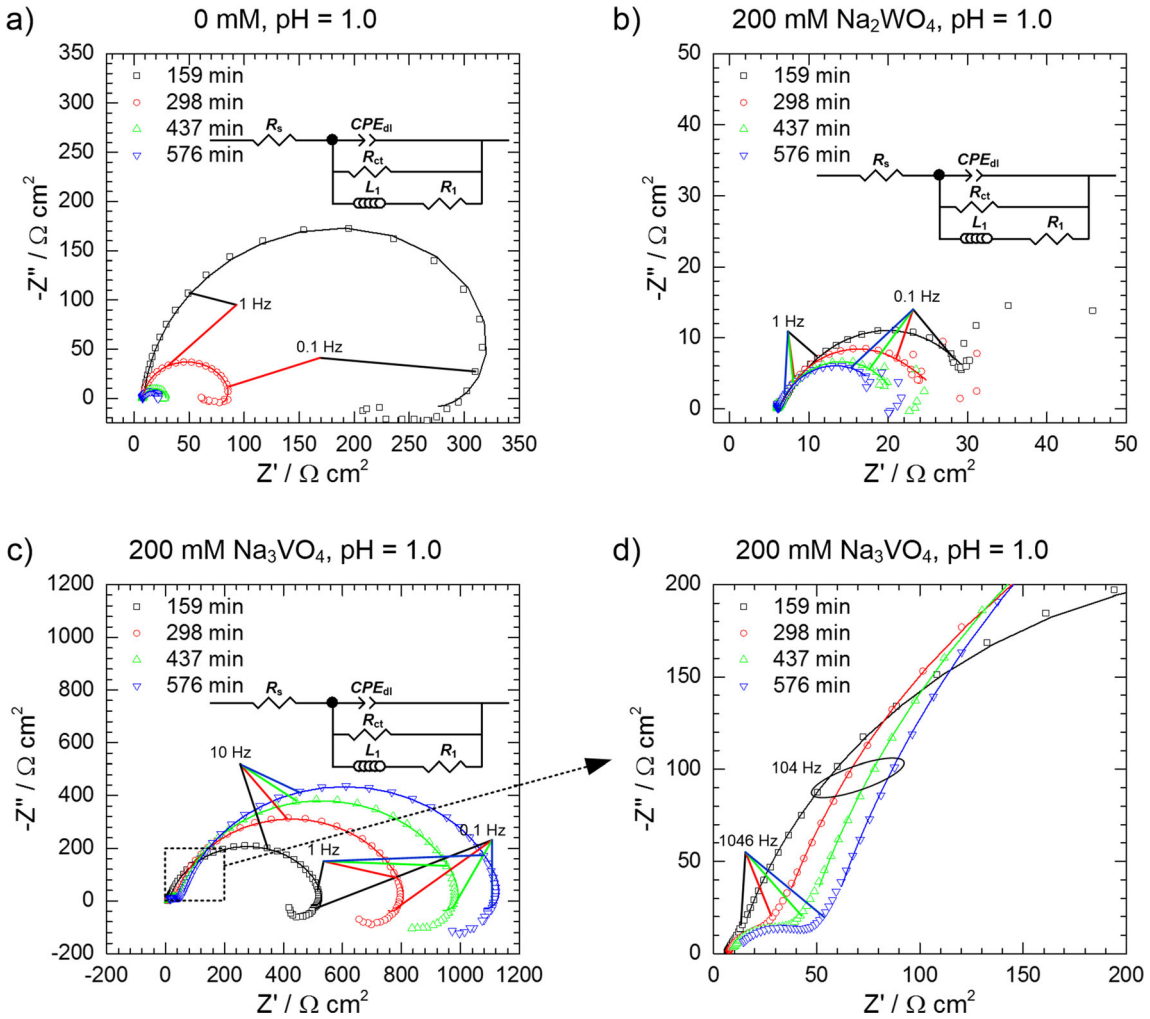

Fig. 8 Nyquist plots for the corrosion of Al_2Cu in 0.5 M H_3PO_4 at pH = 1 and T = 303 K as a function of time and initial concentration of Na_3VO_4 and Na_2WO_4; continuous lines represent an approximation of the obtained data; impedances were multiplied by the geometric surface area

It can be concluded that corrosion inhibition of intermetallic Al_2Cu in the H_3PO_4–Na_3VO_4 system did not occur. The vanadium in the studied solutions, where the pH was between 1 and 4 and its total concentration was between 10 and 200 mM, existed in two forms. The decavanadate $[H_2V_{10}O_{28}]^{4-}$ ion is stable for pH > 2 and a total concentration of vanadium > ca. 10 mM, whereas VO_2^+ occurs in a more acidic solution and lower total V concentration. Upon addition of Na_3VO_4 to 0.5 M H_3PO_4, the solution turned dark red-brown. This indicates the formation of $[HPV_{14}O_{42}]^{9-}$ heteropolyoxovanadate [20]. However, neither the isopolyoxovanadates nor the heteropolyoxovanadates inhibited the corrosion of the Al_2Cu. At a sufficiently acidic solution (pH = 1), the vanadium species were reduced on the surface of the electrode, and probably vanadium(IV) phosphate $VOHPO_4{\cdot}xH_2O$ (x = 0.5, 4) was formed [48]. This result may be useful from the point of view of the preparation of conversion coatings on aluminium alloys.

In the case of sodium tungstate, the formation of heteropolyoxotungstate was confirmed using UV-Vis spectroscopy. The absorption band at ca. 260 nm appeared after dissolution of Na_2WO_4 in 0.5 M H_3PO_4. Thus, $[\alpha\text{-}PW_{12}O_{40}]^{3-}$ was present in the solutions, where the initial concentration of the monometalate was ≤ 100 mM. When the pH of the solution was raised above 1.5–2.0, it was reversibly converted to a lacunary $[\alpha\text{-}PW_{11}O_{39}]^{7-}$ anion, which also has an absorption band at approximately 260 nm [20]. This anion may be responsible for the weak inhibition effect observed for 200 mM of Na_2WO_4 at pH = 2.2. However, the contribution of isopolyoxotungstate species present in the solution cannot be excluded.

Summary

Sodium orthovanadate, sodium tungstate and sodium molybdate were tested as corrosion inhibitors of intermetallic Al_2Cu in 0.5 M H_3PO_4. When their concentration in orthophosphoric acid is too low, severe dealloying of the Al_2Cu phase occurs. The inhibition effect, observed for 0.5 M H_3PO_4/0.2 M

Na_3VO_4 and 0.5 M H_3PO_4/0.2 M Na_2WO_4, is mainly related to the pH increase in the solution to the range, where the corrosion rate of the Al_2Cu phase is low. However, these results do not necessarily exclude the above-mentioned isopolyoxoanions and heteropolyoxoanions as corrosion inhibitors of aluminium alloys in acidic solutions. Their influence on the corrosion behaviour of an Al–Cu solid solution and other intermetallics in H_3PO_4 should also be studied. Sodium orthovanadate seems to be the least likely to replace CrO_3 in stripping solutions for anodic coatings, since precipitation of insoluble salts during etching negatively affects the gravimetric determination of the coating weight.

Acknowledgments The authors gratefully acknowledge Dr. Dariusz Szeliga and Mr. Andrzej Gradzik for preparing the Al_2Cu intermetallic phase, Dr. Barbara Kościelniak for her help in microscopic analysis, Mr. Andrzej Obłój for his help in conducting the electrochemical research and Prof. Andrzej Lasia for his help in interpretation of EIS data and valuable comments.

Funding information The National Science Centre, Poland, Grant No. 2016/23/D/ST5/01343 provided financial support.

References

1. Belov NA, Eskin DG, Aksenov AA (2005) Multicomponent phase diagrams: applications for commercial aluminum alloys. Elsevier, Oxford
2. Scully JR, Knight TO, Buchheit RG, Peebles DE (1993) Electrochemical characteristics of the Al_2Cu, Al_3Ta and Al_3Zr intermetallic phases and their relevancy to the localized corrosion of Al alloys. Corros Sci 35(1-4):185–195
3. Buchheit RG (1995) A compilation of corrosion potentials reported for intermetallic phases in aluminum alloys. J Electrochem Soc 142(11):3994–3996
4. Osório WR, Spinelli JE, Ferreira IL, Garcia A (2007) The roles of macrosegregation and of dendritic array spacings on the electrochemical behavior of an Al–4.5 wt% Cu alloy. Electrochim Acta 52(9):3265–3273
5. Osório WR, Spinelli JE, Freire CMA, Cardona MB, Garcia A (2007) The roles of Al_2Cu and of dendritic refinement on surface corrosion resistance of hypoeutectic Al-Cu alloys immersed in H_2SO_4. J Alloys Compd 443(1-2):87–93
6. Al-Rawajfeh AE, Al Qawabah SMA (2009) Investigation of copper addition on the mechanical properties and corrosion resistance of commercially pure aluminium. Emirates J Eng Res 14:47–52
7. Osório WR, Siqueira CA, Santos CA, Garcia A (2011) The correlation between electrochemical corrosion resistance and mechanical strength of As-cast Al-Cu and Al-Si alloys. Int J Electrochem Sci 6:6275–6289
8. Özay Ç, Gencer EB, Gökçe A (2018) Microstructural properties of sintered Al – Cu – Mg – Sn alloys. J Therm Anal Calorim 5:23–33
9. Bonatti RS, Meyer YA, Bortolozo AD, Costa D, Wislei R (2019) Morphology and size effects on densification and mechanical behavior of sintered powders from Al-Si and Al-Cu casting alloys. J Alloys Compd 786:717–732
10. Lebouil S, Tardelli J, Rocca E, Volovitch P, Ogle K (2014) Dealloying of Al_2Cu, Al_7Cu_2Fe, and Al_2CuMg intermetallic phases to form nanoparticulate copper films. Mater Corros 65(4):416–424
11. Sheasby PG, Pinner R, Wernick S (2001) The surface treatment and finishing of aluminium and its alloys. ASM International, Trowbridge
12. ASTM B137–95 (2009) Standard test method for measurement of coating mass per unit area on anodically coated aluminum. ASTM International, West Conshohocken PA
13. Iannuzzi M, Frankel GS (2007) Mechanisms of corrosion inhibition of AA2024-T3 by vanadates. Corros Sci 49(5):2371–2391
14. Ralston KD, Chrisanti S, Young TL, Buchheit RG (2008) Corrosion inhibition of aluminum alloy 2024-T3 by aqueous vanadium species. J Electrochem Soc 155(7):C350–C359
15. Ralston KD, Young TL, Buchheit RG (2009) Electrochemical evaluation of constituent intermetallics in aluminum alloy 2024-T3 exposed to aqueous vanadate inhibitors. J Electrochem Soc 156(4):C135–C146
16. Ralston KD, Buchheit RG (2013) An initial exploration of corrosion inhibition of AA6061 and AA7075 by aqueous vanadates. ECS Electrochem Lett 2(9):C35–C38
17. Kharitonov DS, Sommertune J, Örnek C, Ryl J, Kurilo II, Claesson PM, Pan J (2018) Corrosion inhibition of aluminium alloy AA6063-T5 by vanadates: local surface chemical events elucidated by confocal Raman micro-spectroscopy. Corros Sci 148:237–250
18. El Abedin SZ (2001) Role of chromate, molybdate and tungstate anions on the inhibition of aluminium in chloride solutions. J Appl Electrochem 31(6):711–718
19. Abd El Aal EE, Abd El Wanees S, Farouk A, Abd El Haleem SM (2013) Factors affecting the corrosion behaviour of aluminium in acid solutions: II. Inorganic additives as corrosion inhibitors for Al in HCl solutions. Corros Sci 68:14–24
20. Pope MT (1983) Heteropoly and isopoly oxometalates. Springer-Verlag, Berlin
21. Krebs B, Tytko KH, Mehmke J, Stiller S (1991) Structure and bonding in the high molecular weight isopolymolybdate ion, $[Mo_{36}O_{112}(H2O)_{16}]^{8-}$. The crystal structure of $Na_8[Mo_{36}O_{112}(H_2O)_{16}].58H_2O$. Eur J Solid State Inorg Chem 28:883–903
22. Müller A, Krickemeyer E, Meyer J, Bögge H, Peters F, Plass W, Diemann E, Dillinger S, Nonnenbruch F, Randerath M (1995) $[Mo_{154}(NO)_{14}O_{420}(OH)_{28}(H_2O)_{70}]^{(25\pm5)-}$: ein wasserlösliches Riesenrad mit mehr als 700 Atomen und einer relativen Molekülmasse von ca. 24000. Angew Chemie 107(19):2293–2295
23. Müller A, Botar B, Das SK, Bögge H, Schmidtmann M, Merca A (2004) On the complex hedgehog-shaped cluster species containing 368 Mo atoms: simple preparation method, new spectral details and information about the unique formation. Polyhedron 23(15):2381–2385
24. Li X, Deng S, Fu H (2011) Sodium molybdate as a corrosion inhibitor for aluminium in H_3PO_4 solution. Corros Sci 53(9):2748–2753
25. Badawy WA, Al-Kharafi FM (1997) The inhibition of the corrosion of Al, Al-6061 and Al-Cu in chloride free aqueous media: I. passivation in acid solutions. Corros Sci 39(4):681–700
26. Nagul EA, McKelvie ID, Worsfold P, Kolev SD (2015) The molybdenum blue reaction for the determination of orthophosphate revisited : opening the black box. Anal Chim Acta 890:60–82
27. Kwolek P, Kamiński A, Dychtoń K, Drajewicz M, Sieniawski J (2016) The corrosion rate of aluminium in the orthophosphoric acid

solutions in the presence of sodium molybdate. Corros Sci 106: 208–216
28. Dychtoń K, Kwolek P (2018) The replacement of chromate by molybdate in phosphoric acid-based etch solutions for aluminium alloys. Corros Eng Sci Technol 53(3):234–240
29. Kwolek P, Wojnicki M (2018) Spectrophotometric study of corrosion inhibition of aluminium in orthophosphoric acid aqueous solutions by using sodium molybdate. Corros Eng Sci Technol 54: 199–204
30. Kwolek P, Pustuła A, Nowak WJ (2019) Influence of molybdophosphoric acid on the kinetics of the anodic coating dissolution. Surf Coatings Technol 357:535–542
31. Boukamp B (1995) A linear Kronig-Kramers transform test for emittance data validation. J Electrochem Soc 142(6):1885–1894
32. Boukamp B (2004) Electrochemical impedance spectroscopy in solid state ionics: recent advances. Solid State Ionics 169(1-4):65–73
33. Birbilis N, Buchheit RG (2008) Investigation and discussion of characteristics for intermetallic phases common to aluminum alloys as a function of solution pH. J Electrochem Soc 155(3):C117–C126
34. Tran A-T, Huet F, Ngo K, Rousseau P (2011) Artefacts in electrochemical impedance measurement in electrolytic solutions due to the reference electrode. Electrochim Acta 56:8034–8039
35. Frateur I, Deslouis C, Orazem ME, Tribollet B (1999) Modeling of the cast iron/drinking water system by electrochemical impedance spectroscopy. Electrochim Acta 44(24):4345–4356
36. Park JJ, Pyun S II (2003) Analysis of impedance spectra of a pitted Inconel alloy 600 electrode in chloride ion-containing thiosulfate solution at temperatures of 298-573 K. J Solid State Electrochem 7(6):380–388
37. Chen L, Lasia A (1992) Study of the kinetics of hydrogen evolution reaction on nickel-zinc powder electrodes. J Electrochem Soc 139(11):3214–3219
38. Chen L, Lasia A (1993) Ni-Al powder electrocatalyst for hydrogen evolution. J Electrochem Soc 140(9):2464–2473
39. Pyun S-I, Shin H-C, Lee J-W, Go J-Y (2012) Electrochemistry of insertion materials for hydrogen and lithium. Springer-Verlag, Berlin
40. Lasia A (2014) Electrochemical impedance spectroscopy and its applications. Springer, New York
41. Ma H, Cheng X, Li G, Chen S, Quan Z, Zhao S, Niu L (2000) The influence of hydrogen sulfide on corrosion of iron under different conditions. Corros Sci 42(10):1669–1683
42. Hirschorn B, Orazem ME, Tribollet B, Vivier V, Frateur I, Musiani M (2010) Determination of effective capacitance and film thickness from constant-phase-element parameters. Electrochim Acta 55(21): 6218–6227
43. Łosiewicz B, Jurczakowski R, Lasia A (2017) Kinetics of hydrogen underpotential deposition at iridium in sulfuric and perchloric acids. Electrochim Acta 225:160–167
44. Cao C (1990) On the impedance plane displays for irreversible electrode reactions based on the stability conditions of the steady state II. Two state variables besides electrode potential. Electrochim Acta 35(5):837–844
45. Umoren SA, Li Y, Wang FH (2010) Effect of polyacrylic acid on the corrosion behaviour of aluminium in sulphuric acid solution. J Solid State Electrochem 14(12):2293–2305
46. Arutunow A, Darowicki K (2009) Impact of sensitization on dissolution process of AISI 304 stainless steel during intergranular corrosion evaluated using DEIS technique. J Solid State Electrochem 13(11):1687–1694
47. Rajan V, Neelakantan L (2017) On the corrosion behavior of Al_2Cu by local electrochemical impedance spectroscopy using droplet cell microscopy. J Solid State Electrochem 21(2):603–609
48. Dummer NF, Bartley JK, Hutchings GJ (2011) Vanadium phosphate materials as selective oxidation catalysts. Adv Catal 54: 189–247